remote sensing

Technical Note

The Time Difference of Arrival Estimation Method Utilizing an Inexact Reconstruction Within the Framework of Compressed Sensing

Shanhe Wang *, Yu Xiang, Yuanyuan Gao, Yu Hua, Changjiang Huang and Xian Zhao

National Time Service Center, Chinese Academy of Sciences, No. 3, Shuyuan East Road, Lintong District, Xi'an 710600, China; xy@ntsc.ac.cn (Y.X.); gaoyy@ntsc.ac.cn (Y.G.); hy@ntsc.ac.cn (Y.H.); huangcj@ntsc.ac.cn (C.H.); zhaoxian@ntsc.ac.cn (X.Z.)
* Correspondence: wangshanhe@ntsc.ac.cn

Abstract: The time difference of arrival (TDOA) estimation plays a crucial role in emitter localization and time synchronization applications. When time among multiple sensors is synchronized, the TDOAs between the sensors and the emitter can be measured to achieve hyperbolic positioning of the emitter. Conversely, if the positions of both the sensors and the emitter are known, TDOAs can be utilized to synchronize the clocks across the sensors. Given that compressed sensing (CS) can reduce both the sampling rate and data volume, thereby enhancing the efficiency of TDOA estimation, there has been growing interest among researchers in exploring TDOA estimation within the CS framework. In scenarios such as passive positioning, the signals received by sensors are often non-cooperative, and the underlying signal system is unknown, making it difficult to obtain a sparse representation of the signal. This paper introduces an incomplete reconstruction-based TDOA estimation method along with an improved variant. By selecting a partial Fourier transform matrix as the measurement matrix and a Fourier transform matrix as the projection matrix, the orthogonal matching pursuit (OMP) algorithm is employed to reconstruct the compressed measurement data. Through subsequent processing steps, such as conjugate mirroring, TDOA estimation between two signals can be performed. Although the reconstructed signal may substantially differ from the original, the accuracy of TDOA estimation remains reliable. Simulation results demonstrate that when the signal-to-noise ratio (SNR) of the received signal is at least 0 dB and the compressed sampling length exceeds one-tenth of the original signal length, the TDOA estimation error of the proposed method is nearly identical to that of the cross-correlation method.

Keywords: compressed sensing; time difference of arrival; inexact reconstruction

Citation: Wang, S.; Xiang, Y.; Gao, Y.; Hua, Y.; Huang, C.; Zhao, X. The Time Difference of Arrival Estimation Method Utilizing an Inexact Reconstruction Within the Framework of Compressed Sensing. *Remote Sens.* **2024**, *16*, 4039. https://doi.org/10.3390/rs16214039

Academic Editors: Xuebo Zhang, Jiahua Zhu, Wei Guo, Xiaotao Huang and Hongtu Xie

Received: 27 September 2024
Revised: 25 October 2024
Accepted: 27 October 2024
Published: 30 October 2024

1. Introduction

In the field of signal processing, measuring the time shift between a signal and its delayed version is of considerable importance. For example, in passive localization [1,2] and indoor positioning [3–5], the critical measurement data in many scenarios comprise the time difference of arrival (TDOA) from the transmission or reflection point to two sensors. The more precise the TDOA estimation, the greater the accuracy of the positioning. In time synchronization applications, when the positions of the transmission or reflection point and the two sensors are accurately known, the TDOA measurement, after correcting for distance differences, reflects the clock difference between the local clocks of the two sensors [6]. Similarly, the more accurate the TDOA estimation, the higher the precision of time synchronization.

In practice, TDOA is typically calculated using the cross-correlation function [7,8]. When improving the signal-to-noise ratio (SNR) or bandwidth is not feasible—such as in passive positioning with opportunistic signals—enhancing the accuracy of TDOA estimation necessitates increasing the sampling rate or extending the sampling duration.

However, this approach significantly complicates data sampling, transmission, and storage, particularly when numerous sensors are involved, and the vast amount of data cannot be effectively and promptly transmitted. Consequently, many researchers have proposed the application of compressed sensing techniques to TDOA estimation methods to reduce the volume of sampling data [9–13].

For a signal of length N, denoted as $\boldsymbol{s}$, the measurement result in compressed sensing is given by [14,15]

$$\boldsymbol{y} = \boldsymbol{\Phi}(\boldsymbol{s} + \boldsymbol{n}) + \boldsymbol{e} \tag{1}$$

where $\boldsymbol{\Phi}$ represents the $M \times N$ measurement matrix with $M \ll N$, $\boldsymbol{n}$ represents the additive noise to the signal, and $\boldsymbol{e}$ is the measurement error (noise) at the measurement stage.

TDOA estimation methods based on compressed sensing determine the time difference using a set of measurements $\boldsymbol{y}$ and a measurement matrix $\boldsymbol{\Phi}$. Depending on whether the $\boldsymbol{y}$ is reconstructed, these methods can be broadly classified into two categories.

The first approach involves estimating the TDOA by reconstructing the original signals $\boldsymbol{s_1}$ and $\boldsymbol{s_2}$ from the measurement results $\boldsymbol{y_1}$ and $\boldsymbol{y_2}$ of two sensors, followed by calculating the cross-correlation function. This method requires the signal to have a sparse representation in a specific basis, meaning there must be a projection matrix that renders the signal sparse when projected. There are two primary strategies for designing the projection matrix: one involves constructing a set of orthogonal bases based on the mathematical expression of the signal, ensuring the signal has a sparse representation in this orthogonal basis, which necessitates prior knowledge of the received signal system; the other strategy is to use time-shifted versions of the signal as row vectors to construct a projection matrix. In theory, the received signal's sparsity in this projection matrix is 1, but the constructed matrix is typically not orthogonal. Therefore, this approach demands sufficient prior knowledge of the signal and a high SNR for the received signal; otherwise, significant errors in signal reconstruction can lead to an inaccurate TDOA estimation.

The second approach estimates the TDOA without reconstructing the measurement results $\boldsymbol{y}$. In most cases, since $\boldsymbol{\Phi}$ projects the signal from a high-dimensional space to a lower dimension, the measurement results $\boldsymbol{y}$ may disrupt the time–delay relationship between the original signals $\boldsymbol{s}$, rendering the cross-correlation method ineffective for TDOA estimation from $\boldsymbol{y}$. Cao, H. proposed estimating the TDOA by leveraging the phase relationship between the product of the discrete Fourier transform (DFT) coefficients from each sensor and the unknown TDOA, thereby avoiding reconstruction [15]. The phase of the product of the DFT coefficients is proportional to the unknown TDOA, which can then be estimated. When the TDOA between the two signals is small, accurate estimation can be achieved by progressively narrowing the search range and step size; however, larger TDOAs may introduce significant deviations.

Salari, S. highlighted that when the measurement matrix $\boldsymbol{\Phi}$ is a Hadamard matrix, the signal projection preserves the time–domain relationship of the signal [10], allowing the correlation of the measurement results $\boldsymbol{y}$ from two sensors to yield a TDOA estimate. However, when the TDOA is large, the estimate may suffer from periodic ambiguities, with a period corresponding to the product of the number of rows in the measurement matrix $\boldsymbol{\Phi}$ and the sampling rate.

Another method is that one sensor performs compressed sampling on the signal to obtain $\boldsymbol{y_1}$, and another reference sensor samples the signal at the Nyquist sampling rate to obtain $\boldsymbol{s_2}$. Then, after delaying $\boldsymbol{s_2}$ by a certain time τ, and projecting through the measurement matrix, the measurement result is obtained.

$$\boldsymbol{y_2}(\tau) = \boldsymbol{\Phi}(\boldsymbol{s_2}(\tau)) \tag{2}$$

By employing cross-correlation calculations between $\boldsymbol{y_2}(\tau)$ and $\boldsymbol{y_1}$, an estimate of the TDOA is obtained. A limitation of this approach is that one sensor must sample at the Nyquist rate, and the estimation of the TDOA requires a certain amount of search time [16].

This paper proposes an incomplete reconstruction-based TDOA estimation method and its improved variant, which estimate the TDOA without requiring an exact reconstruction of the original signal from the measurement results $\boldsymbol{y}$. The primary focus of this method lies in the accuracy of the TDOA estimation rather than the reconstruction fidelity, thereby eliminating the need for the signal to possess a sparse representation. Although the reconstructed signal may significantly deviate from the original, the TDOA estimation accuracy remains robust.

2. Methods

2.1. Cross-Correlation Method

Assuming that the TDOA between the signal from the transmission or reflection point to the two sensors is constant over the observation interval, the signal model received by Sensor 1 and Sensor 2 is represented as

$$\begin{cases} x_1(t) = a_1 s(t-\tau_1) + n_1(t) \\ x_2(t) = a_2 s(t-\tau_2) + n_2(t) \end{cases} \tag{3}$$

where $s(t)$ is the signal radiated by the transmission or reflection point, the transmission coefficients a_1 and a_2 represent the attenuation experienced by the signal during its propagation path. τ_1 and τ_2 represent the time delay of the signal from transmission to reception, and $n_1(t)$ and $n_2(t)$ are the additive noise received together with the signal, $x_1(t)$ and $x_2(t)$ represent the received signals of the two sensors, and $[0, T)$ represents the observation interval.

To simplify the signal model, taking the signal received by Sensor 1 as a reference, we have

$$\begin{cases} x_1(t) = s(t) + n_1(t) \\ x_2(t) = as(t-D) + n_2(t) \end{cases} \tag{4}$$

where $a = a_2/a_1$ is the ratio of transmission coefficients, and $D = \tau_2 - \tau_1$ is the time difference between signals. Using digital signal processing methods, Equation (4) is written in discrete form after sampling as

$$\begin{cases} x_1(n) = s(n) + n_1(n) \\ x_2(n) = as(n-D) + n_2(n) \end{cases} \tag{5}$$

where N denotes the number of sampling points. We assume that $s(n)$ is a stationary band-limited zero-mean random signal and the noises $n_1(n)$ and $n_2(n)$ are uncorrelated zero-mean white noise. Moreover, the signal is assumed to be independent of the noises, and the cross-correlation function between signals $x_1(n)$ and $x_2(n)$ can be expressed as

$$\begin{aligned} R_{x_1x_2}(\tau) &= E[x_1(n)x_2(n+\tau)] \\ &= aE[s(n)s(n+\tau-D)] + E[s(n)n_2(n+\tau)] \\ &\quad + aE[n_1(n)s(n+\tau-D)] + E[n_1(n)n_2(t+\tau)] \\ &= aR_{ss}(\tau-D) \end{aligned} \tag{6}$$

where $R_{ss}(\tau) = E[s(n)s(n+\tau)]$ represents the autocorrelation function of $s(t)$.

For the ergodic random process, the statistical cross-correlation function can be replaced by the time cross-correlation function; that is, the biased estimation expression of $R_{x_1x_2}(\tau)$ within the observation time is

$$\hat{R}_{x_1x_2}(\tau) = \frac{1}{N}\sum_{n=0}^{N-|\tau|-1} x_1(n)x_2(n+\tau) \tag{7}$$

According to the properties of the autocorrelation function of a stationary random process, when $s(n)$ is not a periodic signal, for any $\tau \neq 0$, we have

$$|R_{ss}(\tau)| \leq |R_{ss}(0)| \tag{8}$$

Thus, $|R_{x_1x_2}(\tau)| \leq |a| \cdot |R_{ss}(0)| = |R_{x_1x_2}(D)|$, and the parameter τ that maximizes $\left|\hat{R}_{x_1x_2}(\tau)\right|$ is an estimate of the D, denoted as $\hat{D}$; that is,

$$\hat{D} = \arg\{\max(|\hat{R}_{x_1x_2}(\tau)|)\} \tag{9}$$

Based on the above method, many improved algorithms have been derived, such as the generalized cross-correlation method [7,8,17], adaptive filtering algorithms [18,19], cross-power spectral phase method [20,21], wavelet transform method [22], and other methods.

For the above methods and improved methods, under the conditions of given signals, increasing the amount of integrated data and improving the SNR of the received signal can effectively improve the accuracy of the TDOA estimation. However, improving the SNR of the received signal requires increasing the antenna aperture or other hardware costs, and increasing the amount of integrated data requires increasing the sampling rate or sampling time, which will lead to the need for more data storage space and increase the pressure of data transmission.

2.2. IRCS Method

Write Equation (5) in vector form, and then after performing a compressed measurement with the measurement matrix $\mathbf{\Phi}$, we obtain

$$\begin{cases} \boldsymbol{y_1} = \mathbf{\Phi}\boldsymbol{x_1} = \mathbf{\Phi}(\boldsymbol{s_1} + \boldsymbol{n_1}) \\ \boldsymbol{y_2} = \mathbf{\Phi}\boldsymbol{x_2} = \mathbf{\Phi}(a\boldsymbol{s_2} + \boldsymbol{n_2}) \end{cases} \tag{10}$$

where $\boldsymbol{x_i} = [x_i(1), x_i(2), \cdots, x_i(N)]^{\mathrm{T}}$, $\boldsymbol{n_i} = [n_i(1), n_i(2), \cdots, n_i(N)]^{\mathrm{T}}$, $i = 1, 2$, $\boldsymbol{s_1} = [s(1), s(2), \cdots, s(N)]^{\mathrm{T}}$, and $\boldsymbol{s_2}$ is the vector $\boldsymbol{s_1}$ that is delayed or advanced by $|D|$ sampling points. The superscript T indicates the transpose of a vector.

Without loss of generality, assume that $a = 1$, $D \neq 0$, and denote $\boldsymbol{x} = \boldsymbol{s_1} + \boldsymbol{n_1}$, $\Delta\boldsymbol{n_{21}} = \boldsymbol{n_2} - \boldsymbol{n_1}$, with $\boldsymbol{x}^D$ being the vector $\boldsymbol{x}$ that is delayed or advanced by $|D|$ sampling points.

$$\begin{cases} \boldsymbol{y_1} = \mathbf{\Phi}\boldsymbol{x} \\ \boldsymbol{y_2} = \mathbf{\Phi}(\boldsymbol{x}^D + \Delta\boldsymbol{n_{21}}) \end{cases} \tag{11}$$

Let

$$\boldsymbol{\theta} = \mathbf{\Psi}\boldsymbol{x} \ \ or \ \ \boldsymbol{x} = \mathbf{\Psi}^{-1}\boldsymbol{\theta} \tag{12}$$

That is, the projection of $\boldsymbol{x}$ onto the projection matrix $\mathbf{\Psi}$ is denoted as $\boldsymbol{\theta}$. For opportunity signals or non-cooperative signals, such as non-cooperative signals radiated by satellites, the characteristics of the signal are unknown, and the received signal can be considered as a band-limited signal with a fixed frequency as the center frequency. Its power spectral density is relatively continuous with frequency. Therefore, finding a suitable projection matrix $\mathbf{\Psi}$ to make $\boldsymbol{x}$ have sparsity in its projection is very difficult; therefore, most of the time, $\boldsymbol{\theta}$ is not sparse.

Applying the same reconstruction algorithm to the two equations in Equation (11), since $\boldsymbol{\theta}$ is non-sparse. Theoretically, it is impossible to accurately reconstruct the signal, that is, the reconstructed values $\hat{\boldsymbol{\theta}}_{\boldsymbol{1}}$ and $\hat{\boldsymbol{\theta}}_{\boldsymbol{2}}$ differ significantly from $\boldsymbol{\theta}$.

However, if the projection matrix $\mathbf{\Psi}$ is the Fourier transform matrix, then $\boldsymbol{\theta}$ is the Fourier transform of $\boldsymbol{x}$, which represents its spectral information. Rewrite Equation (11) as

$$\begin{cases} \boldsymbol{y_1} = \boldsymbol{A}\boldsymbol{\theta} \\ \boldsymbol{y_2} = \boldsymbol{A}(\boldsymbol{\theta} e^{j\frac{2\pi D}{N}} + \Delta\boldsymbol{\theta_{21}}) \end{cases} \tag{13}$$

where, $\boldsymbol{A} = \mathbf{\Phi}\mathbf{\Psi}^{-1}$, $\Delta\boldsymbol{\theta_{21}} = \mathbf{\Psi}\Delta\boldsymbol{n_{21}}$.

When the measurement matrix $\mathbf{\Phi}$ is a partial Fourier transform matrix, it is composed of M rows that are randomly sampled from the Fourier transform matrix, assuming the row index set is denoted by $\boldsymbol{\kappa}$. In that case, $\boldsymbol{A}$ is a matrix formed by extracting M rows corresponding to $\boldsymbol{\kappa}$ from an $N \times N$ identity matrix. In Equation (13), $\boldsymbol{y_1}$ is a vector composed of M elements selected from $\boldsymbol{\theta}$ corresponding to $\boldsymbol{\kappa}$, which practically means that M components of $\boldsymbol{x}$'s spectrum have been randomly sampled.

$$\boldsymbol{y_1} = [\boldsymbol{\theta}(\boldsymbol{\kappa}(1)), \boldsymbol{\theta}(\boldsymbol{\kappa}(2)), \cdots, \boldsymbol{\theta}(\boldsymbol{\kappa}(M))]^{\mathrm{T}} \tag{14}$$

The reconstruction algorithm selects orthogonal matching pursuit (OMP) algorithm [23], with the number of iterations set to M. Considering the characteristics of A and $\boldsymbol{y_1}$, the k-th ($k \in \boldsymbol{\kappa}$) element of the reconstructed signal $\hat{\boldsymbol{\theta}}_1$ is identical to the k-th element of $\boldsymbol{\theta}$. All other elements of $\hat{\boldsymbol{\theta}}_1$ are zero.

In Figure 1, $\boldsymbol{x}$ is a signal of length 8, $\boldsymbol{\theta}$ is its DFT, $M = 4$, $\boldsymbol{y_1}$ is the measurement result corresponding to $\boldsymbol{\kappa} = \{1, 2, 4, 5\}$, which is composed of the frequency components corresponding to the red line with a dot in $\boldsymbol{\theta}$, and $\hat{\boldsymbol{\theta}}_1$ is the reconstruction result obtained with the OMP algorithm.

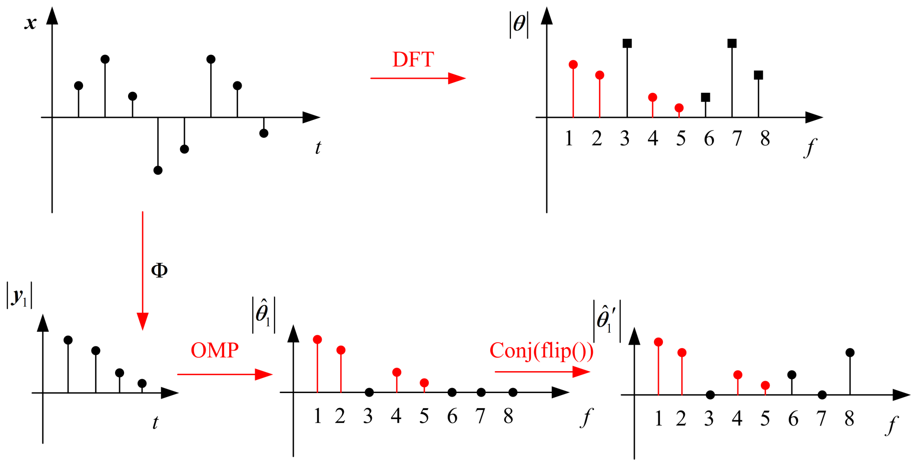

Figure 1. Compressed sampling and reconstruction results.

Similar to $\hat{\boldsymbol{\theta}}_1$, $\hat{\boldsymbol{\theta}}_2$ reconstructed from $\boldsymbol{A}$ and $\boldsymbol{y_2}$ is

$$\hat{\boldsymbol{\theta}}_2 = \hat{\boldsymbol{\theta}}_1 e^{j\frac{2\pi D}{N}} + \Delta\hat{\boldsymbol{\theta}}_{21} \tag{15}$$

where the k-th ($k \in \boldsymbol{\kappa}$) element of $\Delta\hat{\boldsymbol{\theta}}_{21}$ is identical to the k-th element of $\Delta\boldsymbol{\theta}_{21}$. All other elements of $\Delta\hat{\boldsymbol{\theta}}_{21}$ are zero.

Since the reconstructed $\hat{\boldsymbol{\theta}}_1$ and $\hat{\boldsymbol{\theta}}_2$ still retain some of the original signal's frequency and phase information, the cross-correlation function between signals $\boldsymbol{x_1}$ and $\boldsymbol{x_2}$ is

$$\begin{aligned} R^{CS}_{x_1x_2}(\tau) &= IFFT(\hat{\boldsymbol{\theta}}_1 \hat{\boldsymbol{\theta}}_2{}^{*} e^{j\frac{2\pi\tau}{N}}) \\ &= IFFT(\hat{\boldsymbol{\theta}}_1 \hat{\boldsymbol{\theta}}_1{}^{*} e^{j\frac{2\pi(\tau-D)}{N}}) + IFFT(\hat{\boldsymbol{\theta}}_1 \Delta\hat{\boldsymbol{\theta}}_{21}{}^{*} e^{j\frac{2\pi\tau}{N}}) \end{aligned} \tag{16}$$

where $IFFT()$ stands for inverse Fourier transform, and * denotes the complex conjugate.

When $\tau = D$, the first term on the right side of Equation (16) reaches its maximum value. The second term on the right side is the result of the correlation between some components of $\boldsymbol{x_1}$ and some components of the noise $\boldsymbol{n_2} - \boldsymbol{n_1}$. Under the assumption that the signal and noise are uncorrelated, the expectation of this part is approximately 0. Therefore, the TDOA estimate value is

$$\hat{D} = \arg\{\max(|R^{CS}_{x_1x_2}(\tau)|)\} \tag{17}$$

The aforementioned method is referred to as the TDOA estimation method, utilizing an inexact reconstruction within the framework of compressed sensing, abbreviated as IRCS.

2.3. EIRCS Method

According to the definition of the DFT, it can be seen that the first half and the second half of the data in $\boldsymbol{\theta}$ are conjugates of each other. When N is an even number, we have

$$\boldsymbol{\theta}(k) = \boldsymbol{\theta}^*(N - k + 2),\ k \in [2, N/2] \tag{18}$$

This conclusion can also be drawn from $\boldsymbol{\theta}$ in Figure 1. If the received signal $\boldsymbol{x}$ undergoes a DFT before generating the measurement matrix $\boldsymbol{\Phi}$, and the index set $\boldsymbol{\kappa_1}$ is recorded for the $M - 2$ largest elements among the 2nd to $N/2$ elements in $\boldsymbol{\theta}$, let the set $\boldsymbol{\kappa} = \left\{1, \boldsymbol{\kappa_1}, \frac{N}{2} + 1\right\}$. Then, $\boldsymbol{y_1}$ retains a minimum of $M - 2$ largest frequency components of the received signal. Based on the conjugate symmetry of the DFT, the final reconstruction result obtained from $\boldsymbol{y_1}$ is

$$\hat{\boldsymbol{\theta}}_{\boldsymbol{1}}{}' = \begin{bmatrix} \hat{\boldsymbol{\theta}}_{\boldsymbol{1}} \\ conj(flip(\boldsymbol{\theta}^{\kappa_1})) \end{bmatrix} \tag{19}$$

where $conj(flip(\boldsymbol{\theta}^{\kappa_1}))$ is the vector obtained by reversing the order of elements in $\hat{\boldsymbol{\theta}}_{\boldsymbol{1}}(\boldsymbol{\kappa_1})$ and then taking the complex conjugate. As shown by the $\hat{\boldsymbol{\theta}}_{\boldsymbol{1}}{}'$ curve in Figure 1, $\hat{\boldsymbol{\theta}}_{\boldsymbol{2}}{}'$ is similar.

For example, in Figure 1, $\boldsymbol{\kappa} = \{1, 2, 3, 5\}$ (at this time $\boldsymbol{\kappa_1} = \{2, 3\}$), which retains more signal energy compared to a randomly selected $\boldsymbol{\kappa} = \{1, 2, 4, 5\}$, leading to a higher estimation accuracy for the TDOA. This method is called the enhanced TDOA estimation method utilizing inexact reconstruction within the framework of compressed sensing, abbreviated as EIRCS.

Algorithm Procedure:

- Initialization: set the signal sampling duration T or sampling length N, as well as the number of rows M of the measurement matrix $\boldsymbol{\Phi}$.
- Construct a partial Fourier transform matrix as the measurement matrix, where $\boldsymbol{\kappa}$ is random (IRCS) or specified (EIRCS), and extract the corresponding M rows from the $N \times N$ identity matrix to form the sensing matrix $\boldsymbol{A}$.
- Compress the signal according to Equation (10) to obtain the measurement values $\boldsymbol{y_1}$ and $\boldsymbol{y_2}$.
- Select the OMP reconstruction algorithm with M iterations to reconstruct the signal, and then obtain $\hat{\boldsymbol{\theta}}_{\boldsymbol{1}}$ and $\hat{\boldsymbol{\theta}}_{\boldsymbol{2}}$ (IRCS), or $\hat{\boldsymbol{\theta}}_{\boldsymbol{1}}{}'$ and $\hat{\boldsymbol{\theta}}_{\boldsymbol{2}}{}'$ from Equation (19) (EIRCS).
- Estimate the TDOA according to Equation (17).

2.4. Performance Analysis

This section analyzes the IRCS and EIRCS methods in terms of algorithm complexity and Cramér–Rao lower bound (CRLB).

2.4.1. Algorithm Complexity

Algorithm complexity is a critical metric for evaluating the performance of algorithms. In the case of the OMP algorithm, its computational complexity is expressed as $O(kMN)$, where k denotes the sparsity of the reconstructed signal, and M and N represent the number of rows and columns of matrix $\boldsymbol{A}$, respectively. Since the matrix $\boldsymbol{A}$ consists of M rows extracted from an N-dimensional identity matrix, this significantly simplifies many computations.

In the research presented in this paper, we set $k = M$. This allows us to implement the OMP algorithm using a very straightforward method. Taking the reconstruction of signal $\hat{\boldsymbol{\theta}}_{\boldsymbol{1}}$ using matrix $\boldsymbol{A}$ and vector $\boldsymbol{y_1}$ as an example, we first derive $\boldsymbol{\kappa}$ based on the generation of $\boldsymbol{A}$ and generate an $N \times 1$ zero vector $\boldsymbol{b}$. We then initialize the counter $i = 0$ and perform the following steps:

- Compute $i = i + 1$.
- Assign the i-th element of $\boldsymbol{y_1}$ to the $\boldsymbol{\kappa}(i)$-th element of vector $\boldsymbol{b}$.
- Repeat the above steps until $i = M$.

At this point, the vector $\boldsymbol{b}$ becomes the reconstructed signal $\hat{\boldsymbol{\theta}}_{\mathbf{1}}$. The complexity of this algorithm is only $O(M)$, indicating that the OMP algorithm exhibits a very high computational efficiency in the context of the IRCS or EIRCS.

This simplification not only reduces the computational burden but also enhances the algorithm's practical performance when dealing with high-dimensional data. This is particularly important for signal reconstruction problems that require real-time processing and efficient computation. Therefore, we can assert that the IRCS or EIRCS provides an efficient solution for practical applications.

2.4.2. CRLB

When using communication satellites or broadcasting satellites as radiation sources, the signals they emit are generally random non-periodic signals, which may occupy a wide frequency range and include various modulation methods. For example, in digital satellite TV signals, there are signals from multiple channels, with each channel including the amplitude-modulated signal for the TV image and the frequency-modulated signal for the accompanying audio [24]. After source coding and channel coding, these signals approximate random signals. These random signals are very similar to band-limited white noise (BLWN), which is non-sparse in the time domain and remains a non-sparse signal after a Fourier transformation.

Therefore, we select the signal $s(t)$ and noise $n_1(t)$, $n_2(t)$ as zero-mean independent Gaussian BLWN sequences, while denoting the noise variances, and

$$SNR = 10\log_{10}\frac{\sigma_s^2}{\sigma^2} \tag{20}$$

The CRLB of the TDOA estimation is [14,15]

$$CRLB = \frac{3(1+2R)}{N\pi^2 R^2} \tag{21}$$

where $R = 10^{SNR/10}$.

It is noteworthy that the CLRB of the IRCS or EIRCS is not only influenced by the signal's SNR but also closely related to the parameter M. Generally, under the same conditions, the CLRB of the EIRCS is often not greater than that of the IRCS, which provides the EIRCS with certain advantages in specific applications.

When the value of M is large, the reconstructed signal is relatively close to the original signal, leading to a higher degree of similarity between the two. In this case, the CLRB of both the IRCS and EIRCS can be effectively estimated using Equation (21).

Conversely, when the value of M is small, the energy contained in the reconstructed signal from the original signal is relatively low, resulting in a decrease in effective bandwidth. Under these circumstances, the CLRB of both the IRCS and EIRCS is often higher than the values calculated by Equation (21). This phenomenon indicates that a smaller M value may lead to a deterioration in reconstruction performance, adversely affecting the overall quality of the reconstruction.

3. Experiments

This section conducts simulation experiments on the TDOA estimation using cross-correlation (CC), IRCS, and EIRCS methods. It explores the mean squared error (MSE) of the TDOA estimation values over 100 independent trials under a different SNR (with both signal paths having the same SNR) and different compressed sampling numbers M (for the number of rows in the measurement matrix $\mathbf{\Phi}$ of the IRCS and EIRCS methods). The MSE is obtained from averaging 100 independent trials, so that

$$\mathrm{MSE} = \frac{\sum_{i=1}^{100}\left(\hat{\tau}(i) - D\right)^2}{100} \tag{22}$$

where $\hat{\tau}(i)$ is the TDOA estimate of the i trial.

3.1. The MSE with Respect to the SNR

The signal length N is chosen to be 512, $D = 20$, and the SNR range ranges from -10 dB to 30 dB. We explore the MSE of various methods under different SNRs. Figure 2 presents the MSE of the three methods for the TDOA estimation and the CRLB at different SNRs. The horizontal axis represents the signal SNR in dB. For the ease of presentation, the horizontal axis is expressed as $10\log_{10}(\mathrm{MSE})$, with the unit converted to dB (the same below), but this is still referred to as the MSE in this paper. In Figure 2, the values of M are taken in sequence as $M = N/32, N/16, N/8, N/4$. The black dashed line represents the CRLB, the blue line with triangles represents the CC method, the green line with circles represents the IRCS method, and the red line with stars represents the EIRCS method.

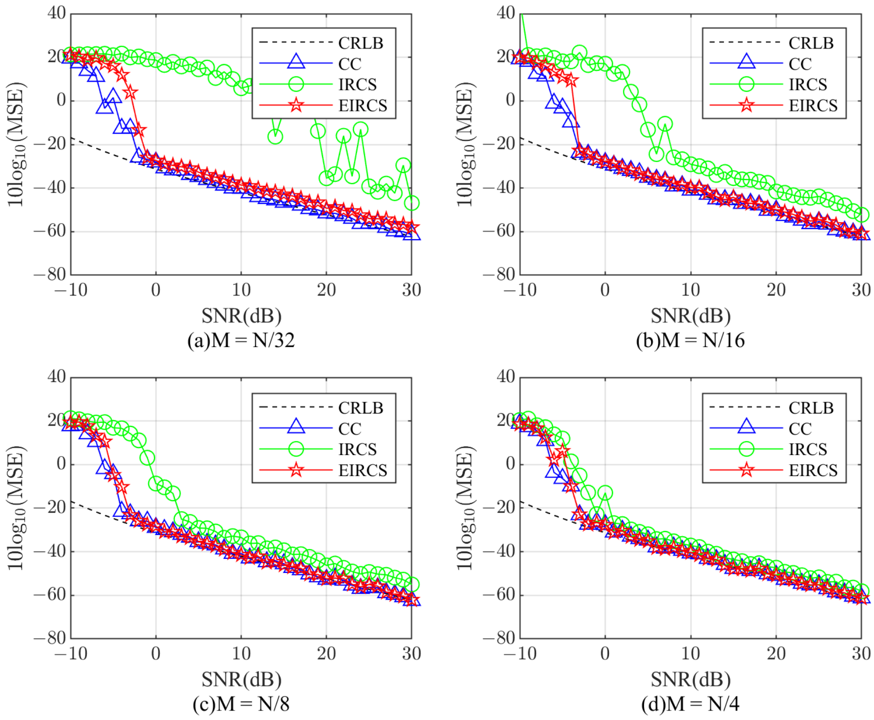

Figure 2. The MSE of the TDOA corresponding to different SNRs.

Figure 2 shows that the MSE of the TDOA estimated by the three methods decreases with the increase in the SNR, and all are above the CRLB curve.

Under the same conditions (SNR > -3 dB), the MSE of CC is generally approximately equal that of the EIRCS, and the EIRCS is less than that of the IRCS. However, as M increases, the IRCS gradually approaches the EIRCS, and the EIRCS gradually approaches CC.

For example, at an SNR of 20 dB, when M takes the values of $N/32$, $N/16$, $N/8$, and $N/4$, the difference in the MSE between the IRCS and EIRCS is 13.8 dB, 8.9 dB, 4.2 dB, and 3.54 dB, respectively, the difference in the MSE between the EIRCS and CC is 2.1 dB, 1.5 dB, 0.3 dB, and 0.01 dB, respectively. When $M = N/2$, the three methods are almost overlapping, which is because the increase in M makes the data used by the three methods to calculate TDOA almost identical.

3.2. The MSE with Respect to the M

At fixed SNRs of -10 dB, 0 dB, 10 dB, and 20 dB, Figure 3 presents the MSE of the TDOA estimation for CC and different M values corresponding to the IRCS and EIRCS methods.

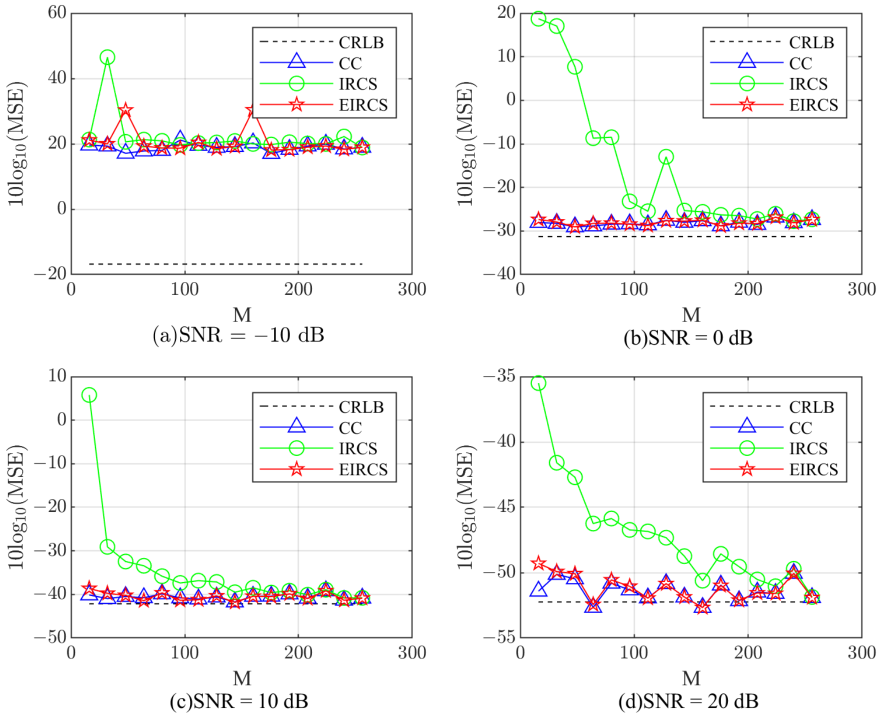

Figure 3. The MSE of the TDOA corresponding to different M values.

Figure 3a indicates that when the SNR is −10 dB, the TDOA estimated from a smaller amount of data has a significant error level. Even at some points, the MSE of the EIRCS exceeds that of the IRCS, such as $M = 48, 160$. The reason is that the noise energy is greater than the true signal. In some cases, the signal reconstructed by the EIRCS method contains more noise relative to the IRCS method, leading to larger time difference estimation errors.

Figure 3b–d show that under the same conditions, the MSE of EIRCS is less than that of IRCS, which also confirms the higher TDOA estimation accuracy of EIRCS mentioned in Section 2.3.

Figure 3 also indicates that when the SNR of the received signal is not lower than 0 dB and $M > 50$ (approximately $N/10$), the performance of the EIRCS is almost identical to CC. This means that despite compressed sensing reducing the sampling data, the estimation accuracy of the TDOA is hardly decreased. In some cases, such as when the SNR = 10 dB and $M = 96$, the MSE of the EIRCS is less than that of CC. This is because the noise is Gaussian white noise, which can be considered to have its spectrum evenly distributed across the signal frequency domain. After reconstruction, most elements of $\hat{\boldsymbol{\theta}}_1$ and $\hat{\boldsymbol{\theta}}_2$ are zero, which can, in some cases, improve the SNR and enhance the accuracy of the TDOA estimation.

Combining Figures 2 and 3, when the SNR is fixed at 0 dB, the CRLB for the TDOA estimation using the IRCS approaches its theoretical value when $M > 100$, and it is significantly greater than the theoretical value when $M < 100$. When the SNR is fixed at 10 dB, M being around 32 is the tipping point where the CRLB approaches and exceeds the theoretical value. Therefore, with different SNRs, the range of M for accurately estimating the CRLB using Equation (21) varies.

4. Conclusions

This paper proposes a TDOA estimation method based on an incomplete reconstruction IRCS and its improved method, EIRCS. Moreover, it provides a brief analysis of their algorithm complexity and the CRLB.

In the IRCS and EIRCS, the measurement matrix $\mathbf{\Phi}$ is a partial Fourier transform matrix, and the projection matrix $\mathbf{\Psi}$ is a Fourier transform matrix. The measurement of the signal is composed of some components of its DFT. After reconstruction using the OMP algorithm, partial frequency information of the signal can be obtained. Although the reconstructed signal differs significantly from the original signal, the TDOA estimation can still be performed. This method does not require a sparse representation of the signal; thus, it has a broader range of application scenarios.

If there is prior knowledge of the signal, by optimizing the generation method of the measurement matrix $\mathbf{\Phi}$, the EIRCS can achieve the same MSE as a traditional cross-correlation method. This is beneficial for reducing the cost of data sampling and storage, improving the efficiency of the TDOA estimation, and it has certain significance for the research of subsequent new methods.

Author Contributions: Conceptualization, S.W. and Y.H.; methodology, S.W.; software, S.W.; validation, Y.X., Y.G. and C.H.; formal analysis, X.Z.; investigation, Y.H.; resources, Y.X.; data curation, Y.G.; writing—original draft preparation, S.W.; writing—review and editing, Y.H.; visualization, Y.G.; supervision, Y.X.; project administration, S.W.; funding acquisition, S.W. All authors have read and agreed to the published version of the manuscript.

Funding: This research was funded by the Basic Research Program of Natural Sciences of Shaanxi Province, grant number 2023-JC-QN-0096).

Data Availability Statement: The original contributions presented in the study are included in the article, further inquiries can be directed to the corresponding author.

Acknowledgments: The authors would like to thank all editors and reviewers for their valuable comments and suggestions.

Conflicts of Interest: The authors declare no conflicts of interest.

References

1. Wang, Z.; Hu, D.; Zhao, Y.; Hu, Z.; Liu, Z. Real-Time Passive Localization of TDOA via Neural Networks. *IEEE Commun. Lett.* **2021**, *25*, 3320–3324. [CrossRef]
2. Pine, K.C.; Pine, S.; Cheney, M. The Geometry of Far-Field Passive Source Localization With TDOA and FDOA. *IEEE Trans. Aerosp. Electron. Syst.* **2021**, *57*, 3782–3790. [CrossRef]
3. Xin, J.; Ge, X.; Zhang, Y.; Liang, X.; Li, H.; Wu, L.; Wei, J.; Bu, X. High-Precision Time Difference of Arrival Estimation Method Based on Phase Measurement. *Remote Sens.* **2024**, *16*, 1197. [CrossRef]
4. Xiao, G.; Dong, Q.; Liao, G.; Li, S.; Xu, K.; Quan, Y. High-Precision Joint TDOA and FDOA Location System. *Remote Sens.* **2024**, *16*, 693. [CrossRef]
5. Khalafalla, M.; Jiang, K.; Tian, K.; Feng, H.; Xiong, Y.; Tang, B. Two-Dimensional Target Localization Approach via a Closed-Form Solution Using Range Difference Measurements Based on Pentagram Array. *Remote Sens.* **2024**, *16*, 1370. [CrossRef]
6. Zhao, K.; Zhao, T.; Zheng, Z.; Yu, C.; Ma, D.; Rabie, K.; Kharel, R. Optimization of Time Synchronization and Algorithms with TDOA Based Indoor Positioning Technique for Internet of Things. *Sensors* **2020**, *20*, 6513. [CrossRef] [PubMed]
7. Azaria, M.; Hertz, D. Time delay estimation by generalized cross correlation methods. *IEEE Trans. Acoust. Speech Signal Process.* **1984**, *32*, 280–285. [CrossRef]
8. Knapp, C.Y.; Carter, G.C. The generalized correlation method for estimation of time delay. *IEEE Trans. Acoust. Speech Signal Process.* **2003**, *24*, 320–327. [CrossRef]
9. Cao, H.; Chan, Y.T.; So, H.C. Maximum Likelihood TDOA Estimation From Compressed Sensing Samples Without Reconstruction. *IEEE Signal Process. Lett.* **2017**, *24*, 564–568. [CrossRef]
10. Salari, S.; Chan, F.; Chan, Y.T.; Read, W. TDOA Estimation With Compressive Sensing Measurements and Hadamard Matrix. *IEEE Trans. Aerosp. Electron. Syst.* **2018**, *54*, 3137–3142. [CrossRef]
11. Daponte, P.; De Vito, L.; Picariello, F.; Rapuano, S.; Remondini, E.; Schettini, C.; Tudosa, I. A Compressed-Sensing System for Radio Spectrum Monitoring and Localization of Noncooperative Sources. *IEEE Trans. Instrum. Meas.* **2024**, *73*, 1–11. [CrossRef]
12. Balestrieri, E.; Vito, L.D.; Picariello, F.; Rapuano, S.; Tudosa, I. A TDoA-based Measurement Method for RF Emitters Localization by Exploiting Wideband Compressive Sampling. In Proceedings of the 2020 IEEE International Instrumentation and Measurement Technology Conference (I2MTC), Dubrovnik, Croatia, 25–28 May 2020; pp. 1–6. [CrossRef]
13. Yang, D.; Li, H.; Peterson, G.D.; Fathy, A. Compressive sensing TDOA for UWB positioning systems. In Proceedings of the 2011 IEEE Radio and Wireless Symposium, Phoenix, AZ, USA, 16–19 January 2011; pp. 194–197. [CrossRef]
14. Cao, H.; So, H.; Chan, Y. Optimum time delay estimation for complex-valued stationary signals. *Signal Process.* **2017**, *131*, 434–440. [CrossRef]

15. Cao, H.; Chan, Y.T.; So, H.C. Compressive TDOA Estimation: Cramér–Rao Bound and Incoherent Processing. *IEEE Trans. Aerosp. Electron. Syst.* **2020**, *56*, 3326–3331. [CrossRef]
16. Chan, Y.; Chan, F.; Rajan, S.; Lee, B. Direct estimation of time difference of arrival from compressive sensing measurements. In Proceedings of the 2015 3rd International Workshop on Compressed Sensing Theory and its Applications to Radar, Sonar and Remote Sensing (CoSeRa), Pisa, Italy, 17–19 June 2015; pp. 273–276. [CrossRef]
17. Carter, G.C. Coherence and time delay estimation. *Proc. IEEE* **2005**, *75*, 236–255. [CrossRef]
18. Jelfs, B.; Sun, S.; Ghorbani, K.; Gilliam, C. An Adaptive All-Pass Filter for Time-Varying Delay Estimation. *IEEE Signal Process. Lett.* **2021**, *28*, 628–632. [CrossRef]
19. Liu, B. Generalized Cross-Correlation Delay Estimation Algorithm Based on Improved LMS Adaptive Filtering. In Proceedings of the 2023 3rd International Conference on Mobile Networks and Wireless Communications (ICMNWC), Tumkur, India, 4–5 December 2023; pp. 1–6. [CrossRef]
20. Zhao, Z.; Hou, Z. The generalized phase spectrum method for time delay estimation. *Chin. J. Acoust.* **1985**, *10*, 201–215.
21. Nikias, C.L.; Pan, R. Time delay estimation in unknown Gaussian spatially correlated noise. *Trans. Acoust. Speech Signal Process.* **1988**, *36*, 1706–1714. [CrossRef]
22. Zhang, L.; Deng, Z.; Han, K.; Li, X.; Zhang, C. TDOA Location Algorithm Based on Adaptive Threshold Function Wavelet Transform. In *Lecture Notes in Electrical Engineering, Proceedings of the China Satellite Navigation Conference (CSNC 2022) Proceedings, Beijing, China, 22–25 May 2022*; Springer: Singapore, 2022; pp. 442–451.
23. Tropp, J.; Gilbert, A. Signal recovery from random measurements via orthogonal matching pursuit. *Trans. Inf. Theory* **2007**, *53*, 4655–4666. [CrossRef]
24. Wang, S. Research on High Precision Time Transfer Method Based on Non-Cooperative Satellite. Ph.D. Thesis, National Time Service Center, Chinese Academy of Sciences, Beijing, China, 2021.